Simulation of supersonic combustion phenomena in evolving geometries with Cartesian upwind methods

Ralf Deiterding
Computer Science and Mathematics Division
Oak Ridge National Laboratory
Oak Ridge, Tennessee

SIAM Conference on Computational Science and Engineering
Costa Mesa, California
February 21, 2007

This work is sponsored by the Office of Advanced Scientific Computing Research; U.S. Department of Energy (DOE) and was performed at the Oak Ridge National Laboratory, which is managed by UT-Battelle, LLC under Contract No. DE-AC05-00OR22725. Part of this work was also performed at the California Institute of Technology and was supported by the ASC program of the Department of Energy under subcontract No. B341492 of DOE contract W-7405-ENG-48.

Outline of the talk

- Introduction
  - *Governing equations*
  - *Difficulties in detonation simulation*
- Finite volume scheme
  - *Roe-type upwind scheme*
  - *Constructing a reliable method for detonation simulation*
- Structured adaptive mesh refinement
  - *Berger-Collela SAMR method*
- Embedded boundary treatment
  - *Verification*
- H_2:O_2:Ar detonation simulations in 2d
  - *Regular oscillating structures in purely Cartesian domains*
  - *Regular detonations under transient conditions in pipe bends*
- Fluid-structure interaction with reaction
- Conclusions

Hydrodynamic equations

Euler equations for mixtures

$$\frac{\partial \rho}{\partial t} + \frac{\partial}{\partial x_k}(\rho u_k) = 0$$

$$\frac{\partial}{\partial t}(\rho u_i) + \frac{\partial}{\partial x_k}(\rho u_i u_k + \delta_{ik} p) = 0$$

$$\frac{\partial E}{\partial t} + \frac{\partial}{\partial x_k}(u_k(E+p)) = 0$$

$$\frac{\partial}{\partial t}(\rho Y_i) + \frac{\partial}{\partial x_k}(\rho Y_i u_k) = \dot{m}_i$$

Implicit equation of state

$$\rho h - p - E + \frac{1}{2}\rho u_k u_k = 0$$

Ideal gas law

$$p = \rho \mathcal{R} T \sum_{i=1}^{N} \frac{Y_i}{W_i}$$

Caloric equation

$$h = \sum_{i=1}^{N} h_i(T) Y_i \qquad \text{with}$$

$$h_i(T) = h_i^0 + \int_{T_0}^{T} c_{pi}(T^*) dT^*$$

Chemical kinetics with Arrhenius law

$$\dot{m}_i = W_i \sum_{j=1}^{M} (\nu_{ji}^r - \nu_{ji}^f)[k_j^f \prod_{n=1}^{N} (\frac{\rho_n}{W_n})^{\nu_{jn}^f} - k_j^r \prod_{n=1}^{N} (\frac{\rho_n}{W_n})^{\nu_{jn}^r}]$$

Difficulties in detonation simulations

1. Discontinuous solutions → high-resolution finite volume method with upwinding in all characteristic fields
2. Stiffness of reaction terms, $\Delta t_c << \Delta t \rightarrow$ Numerical decoupling of time operators with method of fractional steps and local time steps Δt_c
3. Extremely high spatial resolution in reaction zone necessary. Discretization of an exact ZND detonation:

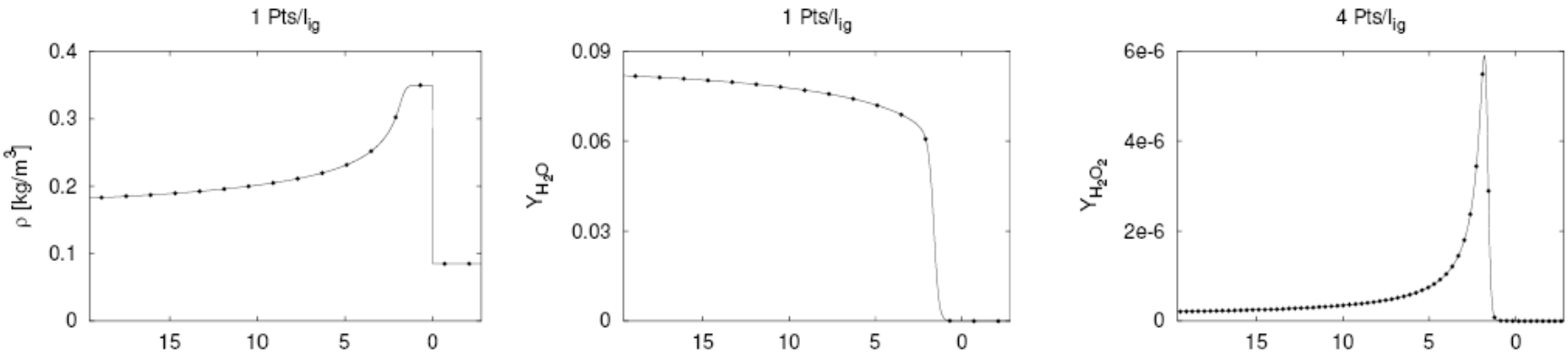

minimal spatial resolution: $7 - 8$ Pts/$l_{ig} \rightarrow \Delta x \approx 0.2 - 0.175$mm

Uniform grids for typical geometries: > 10^7 Pts in 2D, > 10^9 Pts in 3D → Self-adaptive finite volume method (AMR)

4. Problem size even with AMR in 3D enormous → parallelization for massively parallel systems with distributed memory

Finite volume scheme

- Method of fractional steps

$$\mathcal{H}^{(\Delta t)}: \quad \partial_t \mathbf{q} + \nabla \cdot \mathbf{f}(\mathbf{q}) = 0\,, \quad \text{IC: } \mathbf{Q}(t_m) \overset{\Delta t}{\Longrightarrow} \tilde{\mathbf{Q}}$$

$$\mathcal{S}^{(\Delta t)}: \quad \partial_t \mathbf{q} = \mathbf{s}(\mathbf{q})\,, \quad \text{IC: } \tilde{\mathbf{Q}} \overset{\Delta t}{\Longrightarrow} \mathbf{Q}(t_m + \Delta t)$$

1st-order: $\mathbf{Q}(t_m + \Delta t) = \mathcal{S}^{(\Delta t)} \mathcal{H}^{(\Delta t)} (\mathbf{Q}(t_m))$

2nd-order: $\mathbf{Q}(t_m + \Delta t) = \mathcal{S}^{(\frac{1}{2}\Delta t)} \mathcal{H}^{(\Delta t)} \mathcal{S}^{(\frac{1}{2}\Delta t)} (\mathbf{Q}(t_m))$

- Hydrodynamics
  - *Extension to 2d and 3d via dimensional splitting*
  - *Linearized Riemann-solver of Roe-type for thermally perfect gas-mixtures (Grossman, Cinella, J. Comput. Phys. 85, 1990)*
  - *Positivity-preserving*
    - *Switching to HLL for unphysical ρ, p*
    - *Fix for Y_i (Larrouturou, J. Comput. Phys. 95, 1991).*
  - *Entropy fix modification to avoid carbuncle phenomenon (Sanders, Morano, Druguett, J. Comput. Phys. 145, 1998)*
  - *2nd-order MUSCL reconstruction*
- Reaction term
  - *Semi-implicit Runge-Kutta method of 4th order with subcycling (Kaps, Rentrop, Num. Math. 33, 1979)*
  - *Evalutation of m_i with automatically generated optimized Fortran-77 functions in the line of Chemkin-II*
- Evaluation of T with Newton iteration / bisection

Roe's Approximate Riemann Solver

Appropriate matrix $\mathbf{A}(\hat{\mathbf{Q}}) = \mathbf{R}(\hat{\mathbf{Q}})\mathbf{\Lambda}(\hat{\mathbf{Q}})\mathbf{R}^{-1}(\hat{\mathbf{Q}})$

Wave decomposition: $\Delta\mathbf{Q} = \mathbf{Q}_r - \mathbf{Q}_l = \sum_\mu a_\mu \, \hat{\mathbf{r}}_\mu$

$$\mathbf{F}(\mathbf{Q}_l, \mathbf{Q}_r) = \frac{1}{2}\left(\mathbf{f}(\mathbf{Q}_l) + \mathbf{f}(\mathbf{Q}_r) - \sum_\mu |\hat{\lambda}_\mu| \, a_\mu \, \hat{\mathbf{r}}_\mu\right) .$$

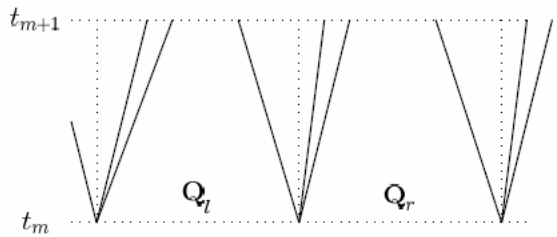

Possible average state for thermally perfect mixtures:

Standard average $\hat{x} = \dfrac{x_l\sqrt{\rho_l} + x_r\sqrt{\rho_r}}{\sqrt{\rho_l} + \sqrt{\rho_r}}$ for $\hat{\rho}$, $\hat{u}_n$, $\hat{H}$, $\hat{W}$, $\hat{T}$, $\hat{h}_i$, $\hat{e}_i$, $\hat{Y}_i$, define $\quad \hat{c}_{\{p/v\}i} = \dfrac{1}{T_r - T_l}\displaystyle\int_{T_l}^{T_r} c_{\{p/v\}i}(\tau)\, d\tau$

Harten-Lax-Van Leer (HLL) Approximate Riemann Solver

$$\mathbf{F}_{HLL}(\mathbf{Q}_l, \mathbf{Q}_r) = \begin{cases} \mathbf{f}(\mathbf{Q}_l) \, , & 0 < s_1 \, , \\ \dfrac{s_3\mathbf{f}(\mathbf{Q}_l) - s_1\mathbf{f}(\mathbf{Q}_R) + s_1 s_3(\mathbf{Q}_r - \mathbf{Q}_l)}{s_3 - s_1} \, , & s_1 \le 0 \le s_3 \, , \\ \mathbf{f}(\mathbf{Q}_r) \, , & 0 > s_3 \, , \end{cases}$$

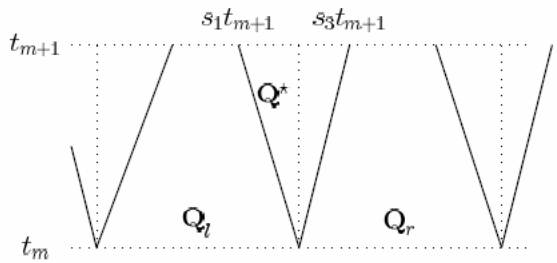

$$s_1 = \min(u_{1,l} - c_l, u_{1,r} - c_r) \, , \quad s_3 = \max(u_{1,l} + c_l, u_{1,r} + c_r)$$

$$\bar{\mathbf{Q}}(x,t) = \begin{cases} \mathbf{Q}_l \, , & x < s_1 \, t \\ \mathbf{Q}^\star \, , & s_1 \, t \le x \le s_3 \, t \\ \mathbf{Q}_r \, , & x > s_3 \, t \end{cases}$$

Switch from Roe to HLL scheme near vacuum state to avoid unphysical values.

Mass Fraction Positivity

Calculate numerical fluxes of partial densities by

$$\mathbf{F}_i^\star = \mathbf{F}_\rho \cdot \begin{cases} Y_i^l \,, & \mathbf{F}_\rho \geq 0 \,, \\ Y_i^r \,, & \mathbf{F}_\rho < 0 \end{cases}$$

to ensure positivity of Y_i.

Example: Mass fraction for a typical Riemann problem after 1 time step with the Roe solver

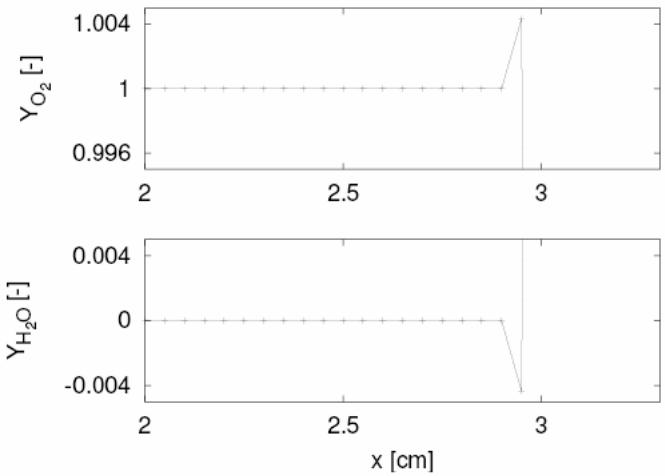

B. Larrouturou. How to preserve the mass fractions positivity when computing compressible multi-component flows. *J. of Comput. Phys.*, 95:59–84, 1991.

Carbuncle Phenomenon

Use 2D modification of entropy correction applied on ALL waves to avoid the carbuncle phenomenon.

Roe HH

Roe EF 3

Exact Riemann solver

SW FVS, VL FVS, HLL, Roe EF 3*

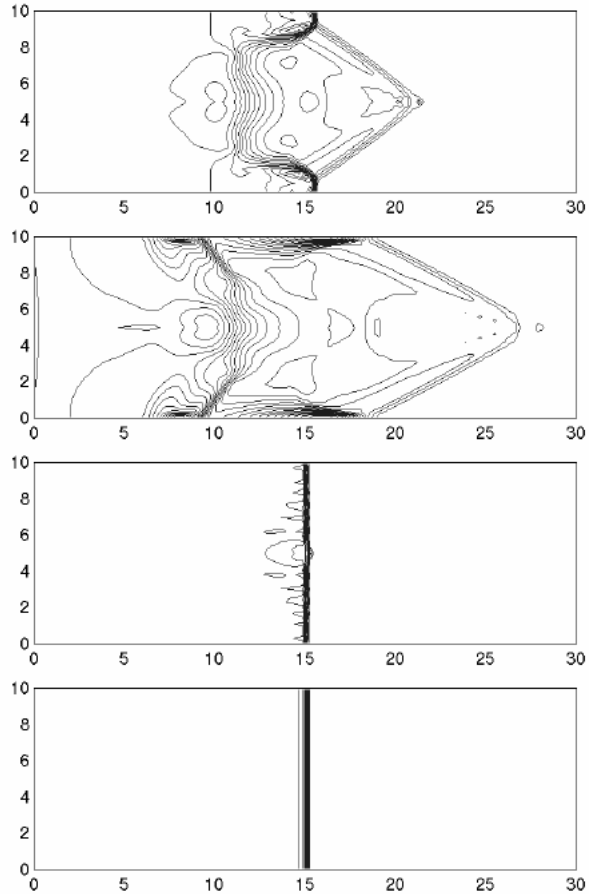

R. Sanders, E. Morano, and M.-C. Druguett. Multidimensional dissipation for upwind schemes: stability and applications to gas dynamics. *J. Comput. Phys.*, 145:511–537, 1998.

A Robust and Reliable Roe-type Scheme

(S1) Calculate standard Roe-averages $\hat{\rho}$, $\hat{u}_n$, $\hat{H}$, $\hat{Y}_i$, $\hat{T}$.

(S2) Compute $\hat{\gamma} := \hat{c}_p/\hat{c}_v$ with $\hat{c}_{\{p/v\}i} = \dfrac{1}{T_r - T_l}\displaystyle\int_{T_l}^{T_r} c_{\{p,v\}i}(\tau)\, d\tau$.

(S3) Calculate $\hat{\phi}_i := (\hat{\gamma}-1)\left(\frac{\hat{\mathbf{u}}^2}{2} - \hat{h}_i\right) + \hat{\gamma}\, R_i\, \hat{T}$ with standard Roe-averages $\hat{e}_i$ or $\hat{h}_i$.

(S4) Calculate $\hat{c} := \left(\sum_{i=1}^{K} \hat{Y}_i\, \hat{\phi}_i - (\hat{\gamma}-1)\hat{\mathbf{u}}^2 + (\hat{\gamma}-1)\hat{H}\right)^{1/2}$.

(S5) Use $\Delta\mathbf{Q} = \mathbf{Q}_r - \mathbf{Q}_l$ and Δp to compute the wave strengths a_m.

(S6) Calculate $\mathbf{W}_1 = a_1\hat{\mathbf{r}}_1$, $\mathbf{W}_2 = \displaystyle\sum_{\iota=2}^{K+d} a_\iota \hat{\mathbf{r}}_\iota$, $\mathbf{W}_3 = a_{K+d+1}\hat{\mathbf{r}}_{K+d+1}$.

(S7) Evaluate $s_1 = \hat{u}_1 - \hat{c}$, $s_2 = \hat{u}_1$, $s_3 = \hat{u}_1 + \hat{c}$.

(S8) Evaluate $\rho^\star_{l/r}$, $u^\star_{1,l/r}$, $e^\star_{l/r}$, $c^\star_{1,l/r}$ from $\mathbf{Q}^\star_l = \mathbf{Q}_l + \mathbf{W}_1$ and $\mathbf{Q}^\star_r = \mathbf{Q}_r - \mathbf{W}_3$.

(S9) If $\rho^\star_{l/r} \le 0$ or $e^\star_{l/r} \le 0$ use $F_{HLL}(Q_l, Q_r)$ and go to (S12).

(S10) Entropy correction: Evaluate $|\tilde{s}_\iota|$.

$$\mathbf{F}_{Roe}(\mathbf{Q}_l, \mathbf{Q}_r) = \tfrac{1}{2}\left(\mathbf{f}(\mathbf{Q}_l) + \mathbf{f}(\mathbf{Q}_r) - \sum_{\iota=1}^{3} |\tilde{s}_\iota|\mathbf{W}_\iota\right)$$

(S11) Positivity correction: Replace $\mathbf{F}_i$ by

$$\mathbf{F}^\star_i = \mathbf{F}_\rho \cdot \begin{cases} Y^l_i\,, & \mathbf{F}_\rho \ge 0\,, \\ Y^r_i\,, & \mathbf{F}_\rho < 0\,. \end{cases}$$

(S12) Evaluate maximal signal speed by $S = \max(|s_1|, |s_3|)$.

Possible Entropy corrections

1. Replace $|s_\iota|$ by $|\tilde{s}_\iota|$ only if $s_\iota(\mathbf{Q}_l) < 0 < s_\iota(\mathbf{Q}_r)$.
2. $|\tilde{s}_\iota| = \begin{cases} |s_\iota| & \text{if} |s_\iota| \ge 2\eta \\ \frac{|s^2_\iota|}{4\eta} + \eta & \text{otherwise} \end{cases}$

   $\eta = \frac{1}{2}\max_\iota \left\{|s_\iota(\mathbf{Q}_r) - s_\iota(\mathbf{Q}_l)|\right\}$

2D modification of entropy correction:

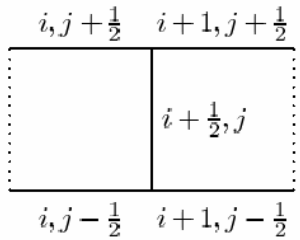

$$\tilde{\eta}_{i+1/2,j} = \max\left\{\eta_{i+1/2,j}, \eta_{i,j-1/2}, \eta_{i,j+1/2}, \eta_{i+1,j-1/2}, \eta_{i+1,j+1/2}\right\}$$

Multi-dimensional Wave Propagation

Use $\mathbf{F}(\mathbf{Q}_l, \mathbf{Q}_r) = \mathbf{f}(\mathbf{Q}_l) + \mathcal{A}^- \Delta\mathbf{Q} = \mathbf{f}(\mathbf{Q}_r) - \mathcal{A}^+ \Delta\mathbf{Q}$ to define fluctuations.

Problem: Need consistent transverse scheme to implement

$$\begin{aligned}
\mathbf{Q}_{jk}^{m+1} = \mathbf{Q}_{jk}^{m} \; & -\tfrac{\Delta t}{\Delta x}\Big(\; \mathcal{A}^- \Delta\mathbf{Q}_{j+\frac{1}{2},k} - \tfrac{1}{2}\tfrac{\Delta t}{\Delta y}\left[\mathcal{A}^-\mathcal{B}^- \Delta Q_{j+1,k+\frac{1}{2}} + \mathcal{A}^-\mathcal{B}^+ \Delta\mathbf{Q}_{j+1,k-\frac{1}{2}}\right] + \\
& \qquad \mathcal{A}^+ \Delta\mathbf{Q}_{j-\frac{1}{2},k} - \tfrac{1}{2}\tfrac{\Delta t}{\Delta y}\left[\mathcal{A}^+\mathcal{B}^- \Delta\mathbf{Q}_{j-1,k+\frac{1}{2}} + \mathcal{A}^+\mathcal{B}^+ \Delta\mathbf{Q}_{j-1,k-\frac{1}{2}}\right]\Big) \\
& -\tfrac{\Delta t}{\Delta y}\Big(\; \mathcal{B}^- \Delta\mathbf{Q}_{j,k+\frac{1}{2}} - \tfrac{1}{2}\tfrac{\Delta t}{\Delta x}\left[\mathcal{B}^-\mathcal{A}^- \Delta\mathbf{Q}_{j+\frac{1}{2},k+1} + \mathcal{B}^-\mathcal{A}^+ \Delta\mathbf{Q}_{j-\frac{1}{2},k+1}\right] + \\
& \qquad \mathcal{B}^+ \Delta\mathbf{Q}_{j,k-\frac{1}{2}} - \tfrac{1}{2}\tfrac{\Delta t}{\Delta x}\left[\mathcal{B}^+\mathcal{A}^- \Delta Q_{j+\frac{1}{2},k-1} + \mathcal{B}^+\mathcal{A}^+ \Delta\mathbf{Q}_{j-\frac{1}{2},k-1}\right]\Big)
\end{aligned}$$

It is not sufficient to implement just (S1)-(S7) for the transverse splitting.

Example: Mass fraction positivity fix

$$\mathbf{F}_i^\star = \mathbf{F}_\rho \cdot \begin{cases} Y_i^l, & \mathbf{F}_\rho \geq 0 \\ Y_i^r, & \mathbf{F}_\rho < 0 \end{cases}$$

Spherical Riemann problem on [0,1]x[0,1]

r=0.2, 3 time steps with CFL=0.45

	Interior	Exterior
ρ	2	1
p	20	1
Y_1	1	0

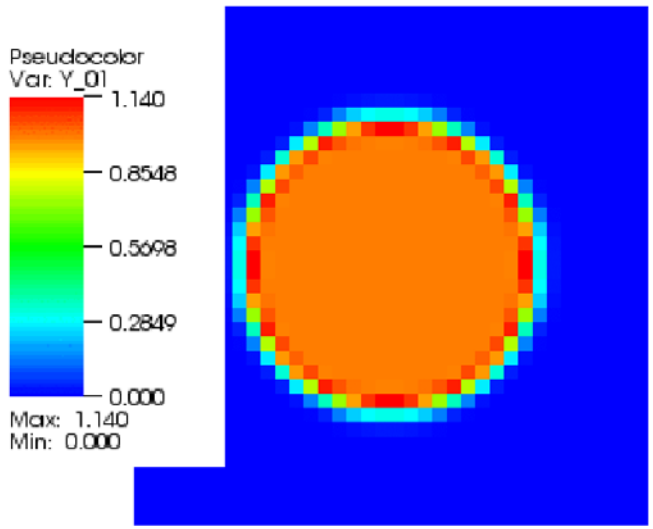

Donor cell method, no correction

Comparison of FV Schemes: MUSCL, Van Albada-limiter

$$\gamma = 1.2,\ E = 50,\ q_0 = 50,\ f = 3.0,\ 40\,\mathrm{Pts}/L_{1/2}$$

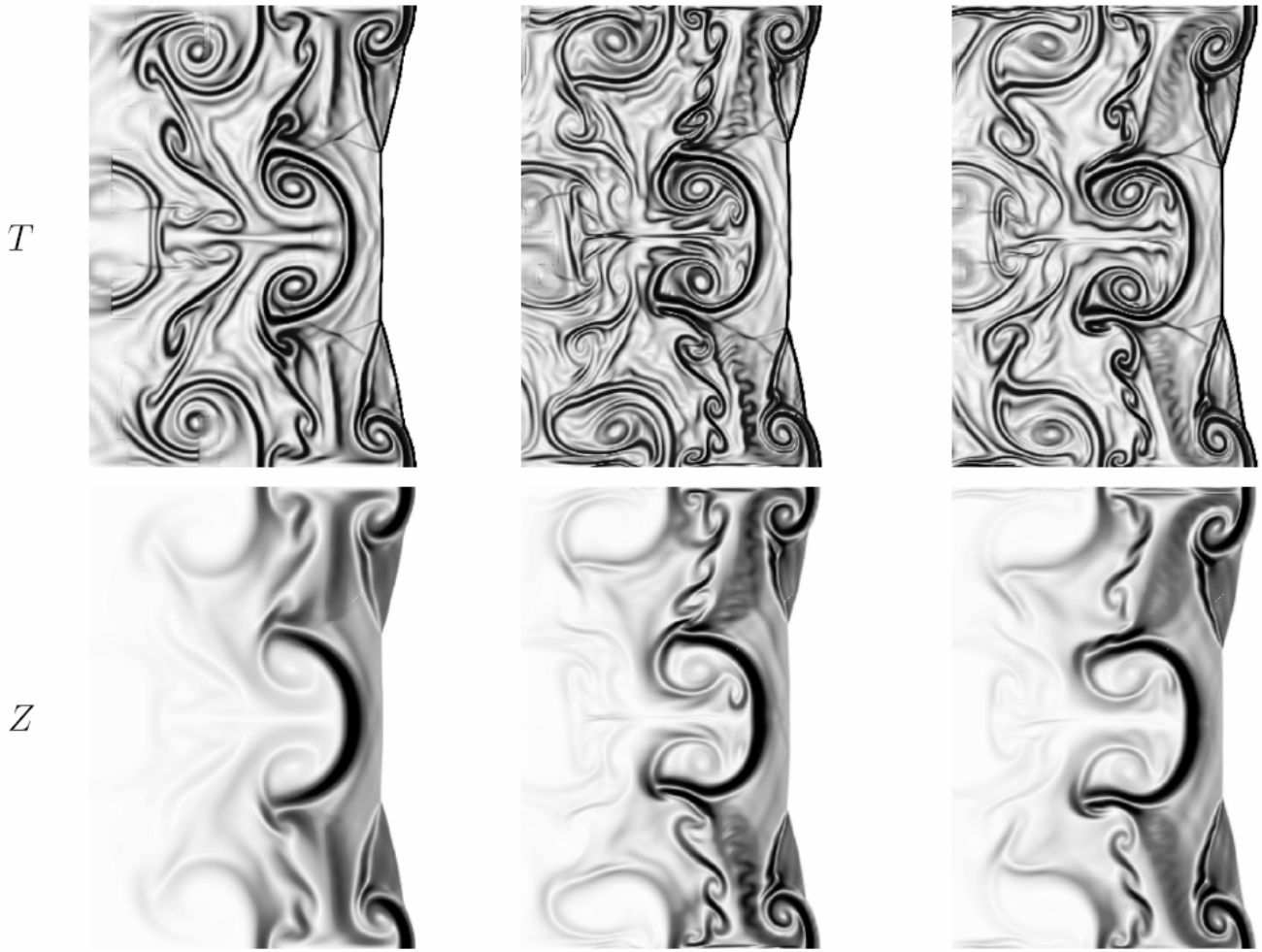

Van Leer FVS, DimSplit

Roe-HLL EF 3*-H, DimSplit

Roe-HLL EF 3*-H, WaveProp

Structured AMR for hyperbolic problems

- For simplicity

$$\partial_t \mathbf{q} + \nabla \cdot \mathbf{f}(\mathbf{q}) = 0$$

- Refined subgrids overlay coarser ones
- Computational decoupling of subgrids by using ghost cells
- Refinement in space *and* time
- Block-based data structures
- Cells without mark are refined
- Cluster-algorithm necessary
- Efficient cache-reuse / vectorization possible
- Explicit finite volume scheme

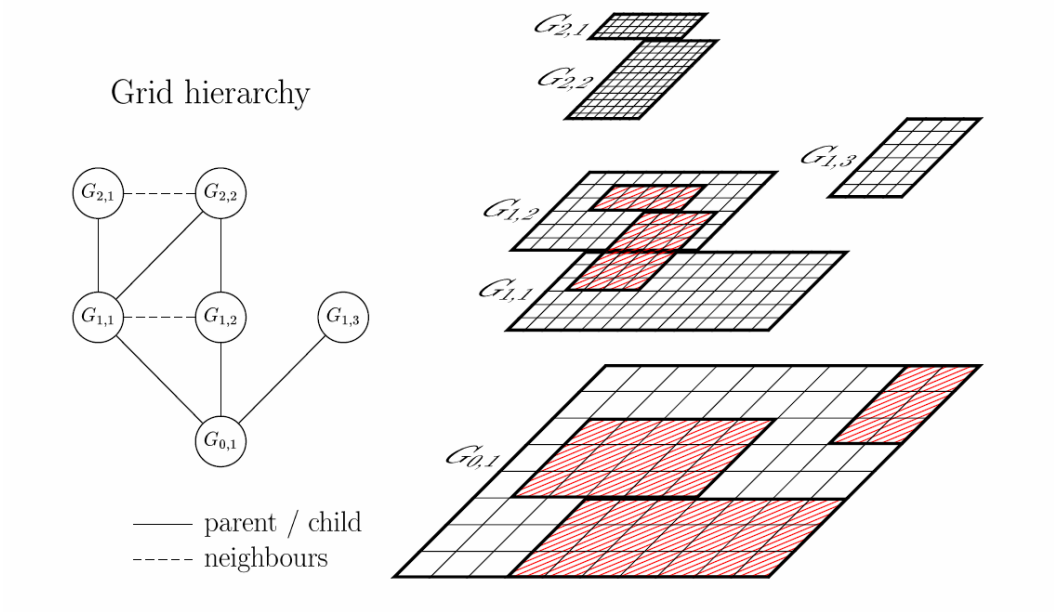

$$\mathbf{Q}_{jk}^{n+1} = \mathbf{Q}_{jk}^{n} - \frac{\Delta t}{\Delta x_1}\left[\mathbf{F}^1_{j+\frac{1}{2},k} - \mathbf{F}^1_{j-\frac{1}{2},k}\right] - \frac{\Delta t}{\Delta x_2}\left[\mathbf{F}^2_{j,k+\frac{1}{2}} - \mathbf{F}^2_{j,k-\frac{1}{2}}\right]$$

only for single rectangular grid necessary

- M. Berger and P. Colella, J. Comput. Phys. 82, 1988.

Berger and Collela SAMR algorithm

Recursive time-stepping method for explicit finite volume scheme

Discretization

$$\mathbf{Q}_{jk}^{n+1} = \mathbf{Q}_{jk}^{n} - \frac{\Delta t}{\Delta x_1}\left[\mathbf{F}^1_{j+\frac{1}{2},k} - \mathbf{F}^1_{j-\frac{1}{2},k}\right] - \frac{\Delta t}{\Delta x_2}\left[\mathbf{F}^2_{j,k+\frac{1}{2}} - \mathbf{F}^2_{j,k-\frac{1}{2}}\right]$$

is applied patch-wise.

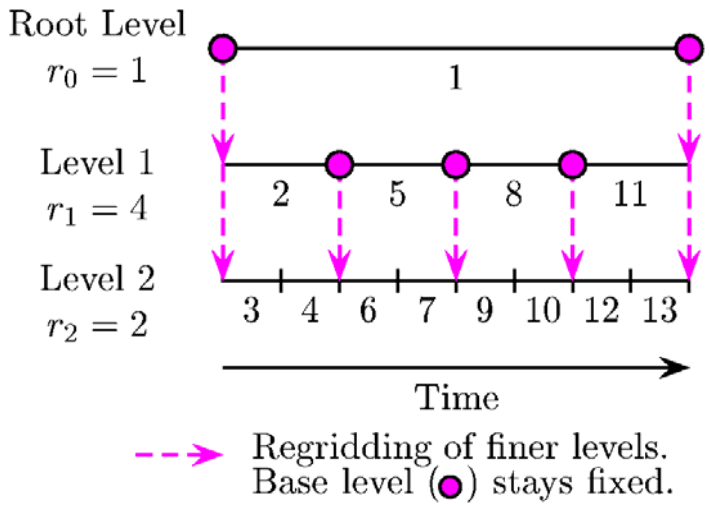

Correction pass:

1. $\delta\mathbf{F}^{1,l+1}_{j-\frac{1}{2},k} := -\mathbf{F}^{1,l}_{j-\frac{1}{2},k}$

2. $\delta\mathbf{F}^{1,l+1}_{j-\frac{1}{2},k} := \delta\mathbf{F}^{1,l+1}_{j-\frac{1}{2},k} + \frac{1}{r_{l+1}}\sum_{\nu=0}^{r_{l+1}-1}\mathbf{F}^{1,l+1}_{v+\frac{1}{2},w+\nu}(t+\mu\Delta t_{l+1})$

3. $\check{\mathbf{Q}}^{l}_{jk}(t+\Delta t_l) := \mathbf{Q}^{l}_{jk}(t+\Delta t_l) + \frac{\Delta t_l}{\Delta x_{1,l}}\delta\mathbf{F}^{1,l+1}_{j-\frac{1}{2},k}$

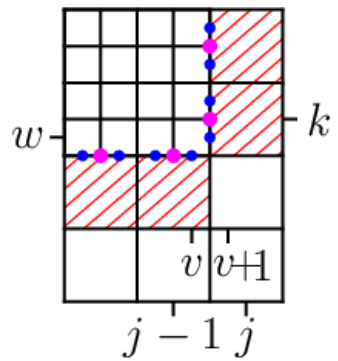

Example: Cell j, k

Parallelization strategy

Domain decomposition: $G_0 = \bigcup_{p=1}^{P} G_0^p$ with $G_0^p \cap G_0^q = \emptyset$ for $p \neq q$

$$G_0^p := \bigcup_{m=1}^{M_0^p} G_{0,m}^p \qquad \longrightarrow \qquad G_l^p := G_l \cap G_0^p$$

Workload: $\mathcal{W}(\Omega) = \sum_{l=0}^{l_{\max}} \left[\mathcal{N}_l(G_l \cap \Omega) \prod_{\kappa=0}^{l} r_\kappa \right]$, $\mathcal{N}_l(G)$ No. of cells on l

Load-balacing: $\mathcal{L}^p := \dfrac{P \cdot \mathcal{W}(G_0^p)}{\mathcal{W}(G_0)} \approx 1$ for all $p = 1, \ldots, P$

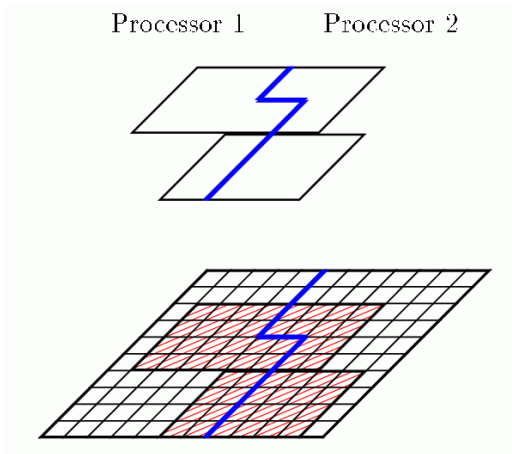

- Data of all levels resides on same node → Interpolation and averaging remain strictly local
- Only parallel operations to be considered:
  - *Parallel synchronization as part of ghost cell setting*
  - *Load-balanced repartitioning of data blocks as part of* **`Regrid(l)`**
  - *Application of flux correction terms on coarse-grid cells*
- Partitioning at root level with generalized Hilbert space-filling curve by M. Parashar

Embedded boundary method

- Incorporate complex moving boundary/ interfaces into a Cartesian solver (extension of work by R.Fedkiw and T.Aslam)
- Implicit boundary representation via distance function φ, normal $n = \nabla\varphi / |\nabla\varphi|$
- Treat an interface as a moving rigid wall
- Method diffuses boundary and is therefore not conservative
- Construction of values in embedded boundary cells by interpolation / extrapolation

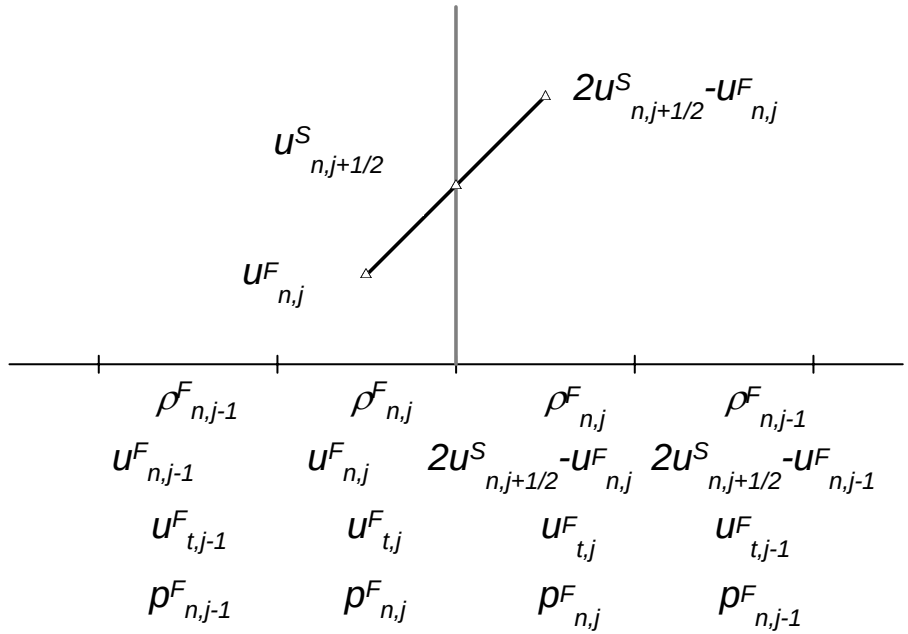

Velocity: $\boldsymbol{u}^F_{Gh} = 2((\boldsymbol{u}^S - \boldsymbol{u}^F_M)\cdot\boldsymbol{n})\,\boldsymbol{n} + \boldsymbol{u}^F_M$

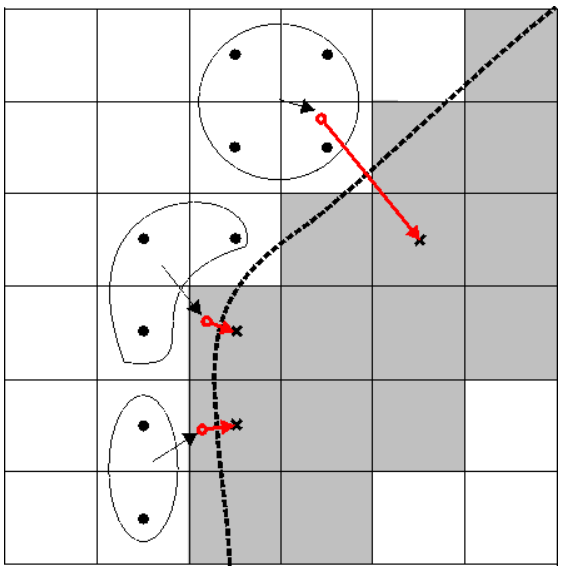

- Higher resolution at embedded boundary required than with first-order unstructured scheme
- Appropriate level-set-based refinement criteria are available to cure deficiencies

GFM Verification – Stationary Vortex

Construct a non-trivial *radially symmetric* and *stationary* solution by balancing hydrodynamic pressure and centripetal force per volume element, i.e.

$$\frac{d}{dr}p(r) = \rho(r)\frac{U(r)^2}{r}, \qquad (1)$$

For $\rho_0 := 1$ and the velocity field

$$U(r) = \alpha \cdot \begin{cases} 2r/R & \text{if } 0 < r < R/2, \\ 2(1 - r/R) & \text{if } R/2 \le r \le R, \\ 0 & \text{if } r > R, \end{cases}$$

We find by integrating Eq. (1) with boundary condition $p(R) = P_0 := 2$ the pressure distribution

$$p(r) = p_0 + 2\rho_0\alpha^2 \cdot \begin{cases} r^2/R^2 + 1 - 2\log 2 & \text{if } 0 < r < R/2, \\ r^2/R^2 + 3 - 4r/R + 2\log(r/R) & \text{if } R/2 \le r \le R, \\ 0 & \text{if } r > R. \end{cases}$$

In Cartesian coordinates the entire solution for Euler equations in primitive variables reads

$$\rho(x,y,t) = \rho_0, \quad u(x,y,t) = -\sin\varphi\, U(r), \quad v(x,y,t) = \cos\varphi\, U(r), \quad p(x,y,t) = p(r)$$

Cartesian accuracy test: $x_c = 0.5, \quad y_c = 0.5, \quad R = 0.4, \quad t_{end} = 1, \quad \Delta h = \Delta x = \Delta y = 1/N, \quad \alpha = R\pi,$

N	Wave Propagation, Roe solver			Godunov-Splitting, Roe solver			WENO - 5 Point			WENO - 7 Point		
	Error	Order	Cost	Error	Order	Cost	Error	Order	Cost	Error	Order	Cost
20	0.0111235		0.0028	0.0182218		0.0029	0.0184102		0.0228	0.0082823		0.0316
40	0.0037996	1.55	0.0091	0.0090662	1.01	0.0086	0.0069655	1.40	0.0875	0.0020886	1.99	0.1430
80	0.0013388	1.50	0.0426	0.0046392	0.97	0.0434	0.0024369	1.52	0.4792	0.0006971	1.58	0.6998
160	0.0005005	1.42	0.1757	0.0023142	1.00	0.1589			1.7320			2.3133

Consistency test for GFM, fixed wall boundary conditions: $\alpha = 0, \quad R_G = R, \quad U_W = R\pi.$

N	Wave Propagation			Godunov-Splitting			WENO - 7 Pt		
	Error	Order	Mass loss	Error	Order	Mass loss	Error	Order	Mass loss
20	1.729e-05		-9.136e-07	3.718e-05		-7.567e-07	3.232e-05		6.297e-06
40	1.646e-05	0.07	-5.025e-08	1.736e-05	1.10	-3.570e-08	2.024e-05	0.68	-2.086e-08
80	5.595e-06	1.56	-2.383e-09	5.702e-06	1.61	-1.190e-09	5.919e-06	1.77	-3.122e-10
160	1.472e-06	1.93	-1.343e-10	1.399e-06	2.03	-9.116e-11			

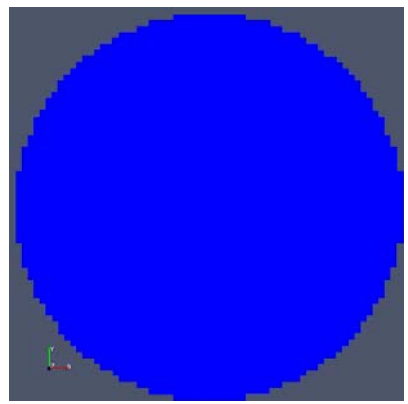

Strong shear flow along embedded boundary: $\alpha = R\pi, \quad R_G = R/2, \quad U_W = 0.$

N	Wave Propagation			Godunov-Splitting			WENO - 7 Pt		
	Error	Order	Mass loss	Error	Order	Mass loss	Error	Order	Mass loss
20	0.0423925		0.0423925	0.0271446		0.0271446	0.0260747		0.0260747
40	0.0358735	0.24	0.0358735	0.0242260	0.16	0.0242260	0.0236603	0.14	0.0236603
80	0.0212340	0.76	0.0212340	0.0128638	0.91	0.0128638	0.0128931	0.88	0.0128931
160	0.0121089	0.81	0.0121089	0.0070906	0.86	0.0070906			

Negligible shear flow along embedded boundary: $\alpha = R\pi, \quad R_G = R, \quad U_W = 0.$

N	Wave Propagation			Godunov-Splitting			WENO - 7 Pt		
	Error	Order	Mass loss	Error	Order	Mass loss	Error	Order	Mass loss
20	0.0120056		0.0079236	0.0144203		0.0020241	0.0064736		0.0028641
40	0.0035074	1.78	0.0011898	0.0073070	0.98	0.0001300	0.0017008	1.93	0.0004790
80	0.0014193	1.31	0.0001588	0.0038401	0.93	-0.0001036	0.0006816	1.32	-5.878e-05
160	0.0005032	1.50	5.046e-05	0.0018988	1.02	-2.783e-06			

Verification of embedded boundary method

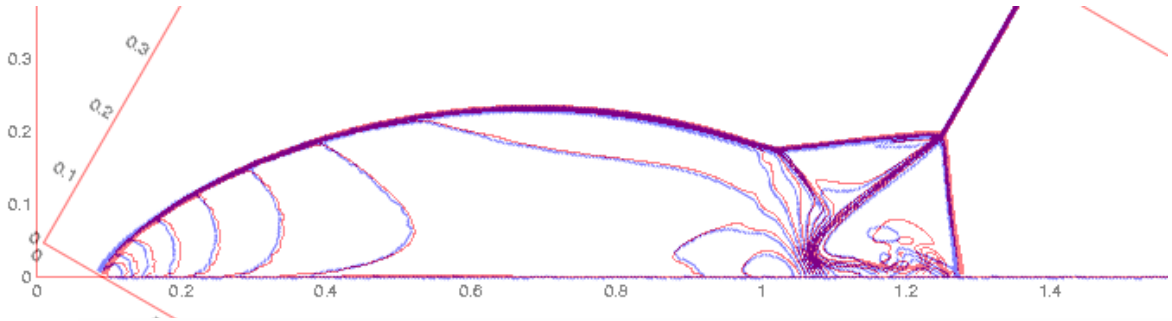

Left: Overlay of two simulation of a double Mach reflection on a 800x400 grid with GFM and 2nd order accurate scheme

Below: Lift-up of a solid body in 2D and 3D when being hit by Mach 3 shock wave, Falcovitz et al. (1997)

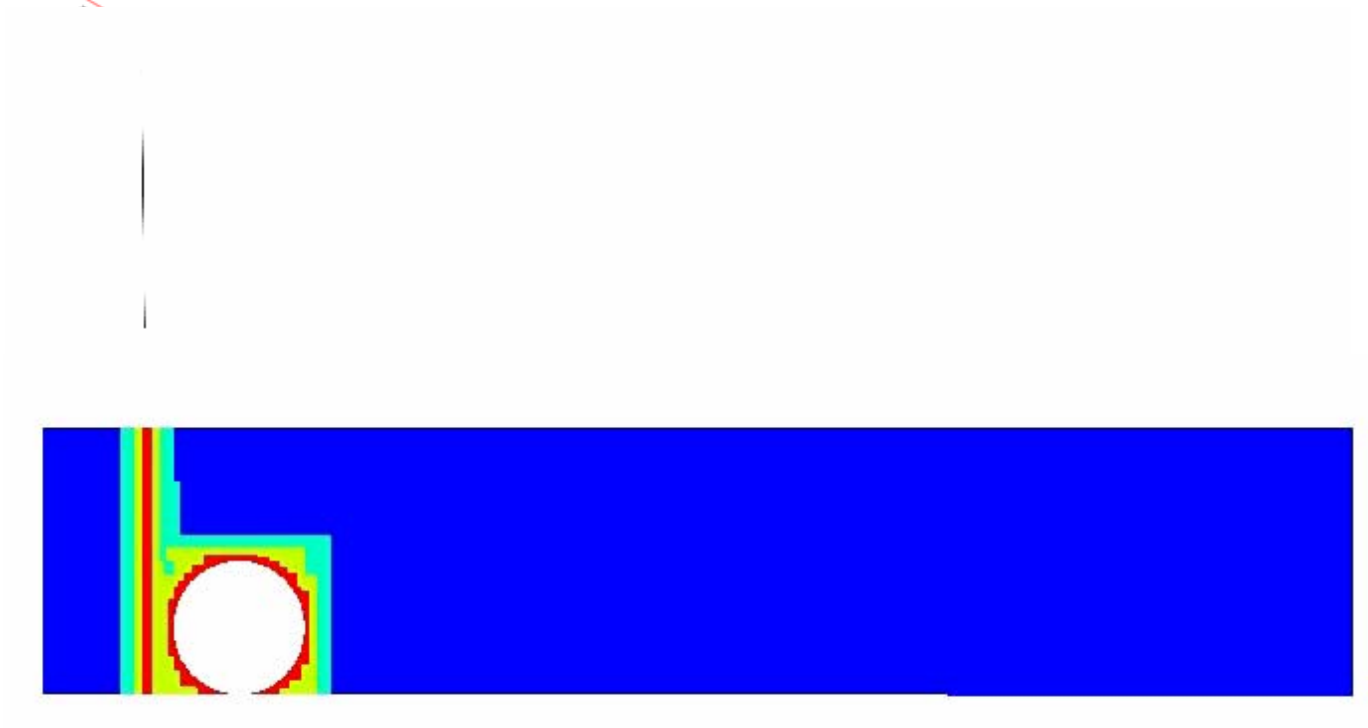

Schlieren plot of density

Refinement Levels

Shock interaction at double-wedge geometry

- Simulation by David Hill (Caltech)
- Mach 9 flow in air hitting a double-wedge (15^o and 45^o)
- Example from Olejniczak, Wright and Candler (JFM 1997)
- AMR base mesh 300x100, 3 additional levels with factor 2
- 3rd order WENO computation vs. 2nd order MUSCL with van Leer flux vector splitting

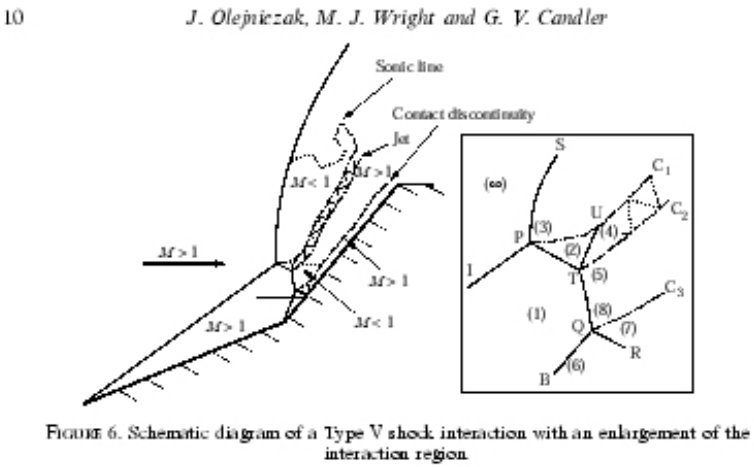

FIGURE 6. Schematic diagram of a Type V shock interaction with an enlargement of the interaction region

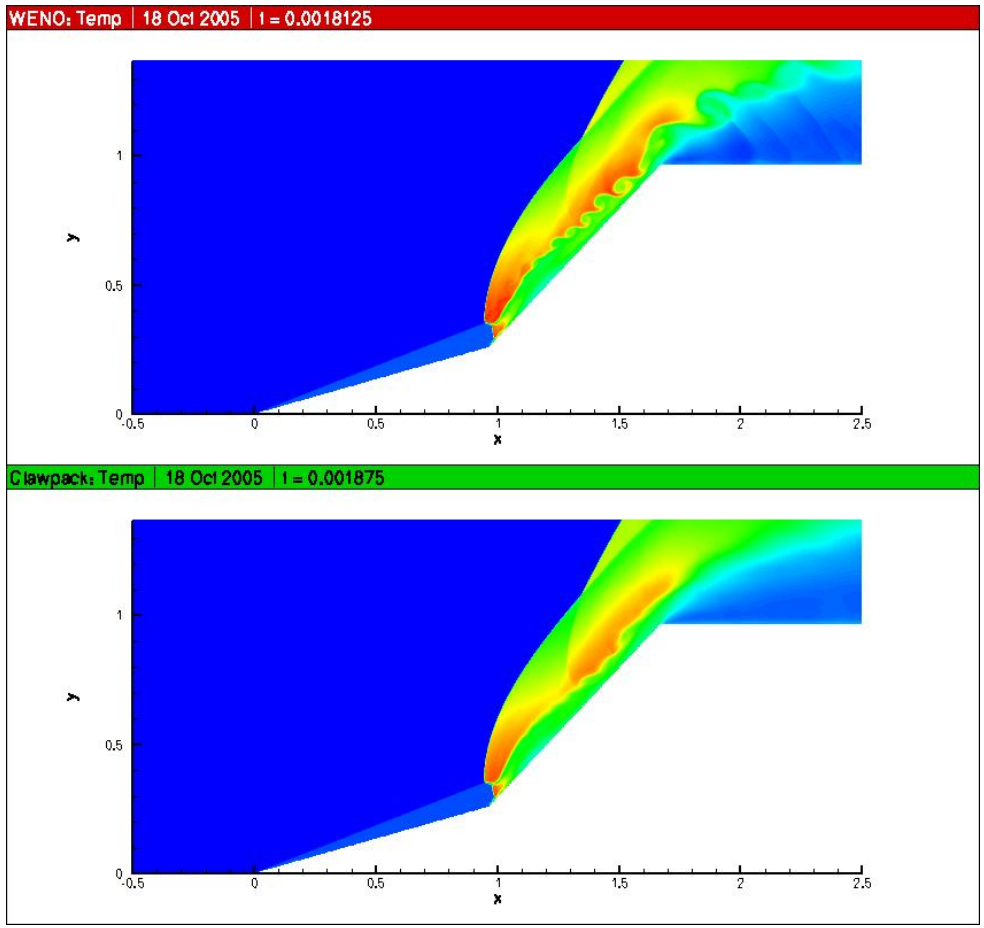

Planar ZND Structure

$H_2 : O_2 : Ar$ Reaction Mechanism

				A [cm, mol, s]	β	E_{act} [cal mol^{-1}]
1.	$H + O_2$	$\longrightarrow$	$O + OH$	1.86×10^{14}	0.00	16790.
2.	$O + OH$	$\longrightarrow$	$H + O_2$	1.48×10^{13}	0.00	680.
3.	$H_2 + O$	$\longrightarrow$	$H + OH$	1.82×10^{10}	1.00	8900.
4.	$H + OH$	$\longrightarrow$	$H_2 + O$	8.32×10^{09}	1.00	6950.
5.	$H_2O + O$	$\longrightarrow$	$OH + OH$	3.39×10^{13}	0.00	18350.
6.	$OH + OH$	$\longrightarrow$	$H_2O + O$	3.16×10^{12}	0.00	1100.
7.	$H_2O + H$	$\longrightarrow$	$H_2 + OH$	9.55×10^{13}	0.00	20300.
8.	$H_2 + OH$	$\longrightarrow$	$H_2O + H$	2.19×10^{13}	0.00	5150.
9.	$H_2O_2 + OH$	$\longrightarrow$	$H_2O + HO_2$	1.00×10^{13}	0.00	1800.
10.	$H_2O + HO_2$	$\longrightarrow$	$H_2O_2 + OH$	2.82×10^{13}	0.00	32790.
11.	$HO_2 + O$	$\longrightarrow$	$OH + O_2$	5.01×10^{13}	0.00	1000.
12.	$OH + O_2$	$\longrightarrow$	$HO_2 + O$	6.46×10^{13}	0.00	56160.
13.	$HO_2 + H$	$\longrightarrow$	$OH + OH$	2.51×10^{14}	0.00	1900.
14.	$OH + OH$	$\longrightarrow$	$HO_2 + H$	1.20×10^{13}	0.00	40100.
15.	$HO_2 + H$	$\longrightarrow$	$H_2 + O_2$	2.51×10^{13}	0.00	700.
16.	$H_2 + O_2$	$\longrightarrow$	$HO_2 + H$	5.50×10^{13}	0.00	57800.
17.	$HO_2 + OH$	$\longrightarrow$	$H_2O + O_2$	5.01×10^{13}	0.00	1000.
18.	$H_2O + O_2$	$\longrightarrow$	$HO_2 + OH$	6.31×10^{14}	0.00	73860.
19.	$H_2O_2 + O_2$	$\longrightarrow$	$HO_2 + HO_2$	3.98×10^{13}	0.00	42640.
20.	$HO_2 + HO_2$	$\longrightarrow$	$H_2O_2 + O_2$	1.00×10^{13}	0.00	1000.
21.	$H_2O_2 + H$	$\longrightarrow$	$HO_2 + H_2$	1.70×10^{12}	0.00	3750.
22.	$HO_2 + H_2$	$\longrightarrow$	$H_2O_2 + H$	7.24×10^{11}	0.00	18700.
23.	$H_2O + M$	$\longrightarrow$	$H + OH + M$	2.19×10^{16}	0.00	105000.
24.	$H + OH + M$	$\longrightarrow$	$H_2O + M$	1.41×10^{23}	−2.00	0.
25.	$H + O_2 + M$	$\longrightarrow$	$HO_2 + M$	1.66×10^{15}	0.00	−1000.
26.	$HO_2 + M$	$\longrightarrow$	$H + O_2 + M$	2.29×10^{15}	0.00	45900.
27.	$H_2O_2 + M$	$\longrightarrow$	$OH + OH + M$	1.20×10^{17}	0.00	45500.
28.	$OH + OH + M$	$\longrightarrow$	$H_2O_2 + M$	9.12×10^{14}	0.00	−5070.
29.	$O + H + M$	$\longrightarrow$	$OH + M$	1.00×10^{16}	0.00	0.
30.	$OH + M$	$\longrightarrow$	$O + H + M$	7.94×10^{19}	−1.00	103720.
31.	$O_2 + M$	$\longrightarrow$	$O + O + M$	5.13×10^{15}	0.00	115000.
32.	$O + O + M$	$\longrightarrow$	$O_2 + M$	4.68×10^{15}	−0.28	0.
33.	$H_2 + M$	$\longrightarrow$	$H + H + M$	2.19×10^{14}	0.00	96000.
34.	$H + H + M$	$\longrightarrow$	$H_2 + M$	3.02×10^{15}	0.00	0.

Third body efficiencies: $f(O_2) = 0.40$, $f(H_2O) = 6.50$

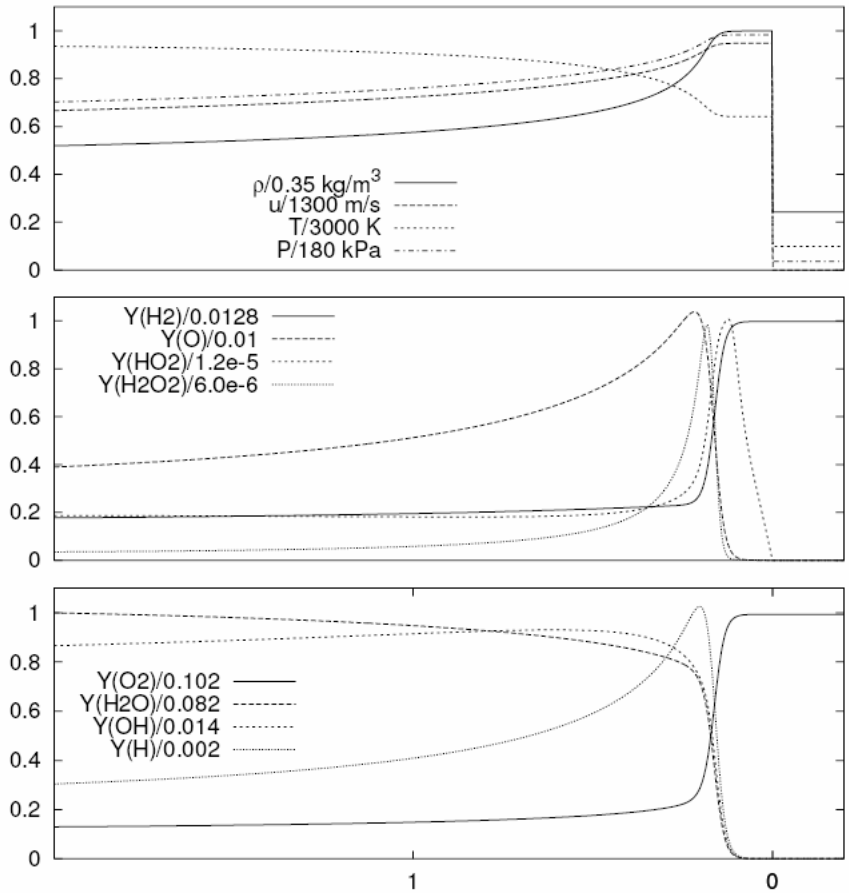

C. K. Westbrook. Chemical kinetics of hydrocarbon oxidation in gaseous detonations. *J. Combustion and Flame*, 46:191–210, 1982.

CJ-detonation of $H_2 : O_2 : Ar$ with molar ratios $2 : 1 : 7$ at $T_0 = 298\,\mathrm{K}$ and $p_0 = 6.67\,\mathrm{kPa}$, $d_{CJ} \approx 1627\,\mathrm{m/s}$. $t_{ig} \approx 3.55\,\mu\mathrm{s}$, $u'_{vN} \approx 395.5\,\mathrm{m/s}$, $l_{ig} \approx 0.14\,\mathrm{cm}$.

Simulation of regular cellular structures

- Regular Chapman-Jouguet detonation for $H_2 : O_2 : Ar/2 : 1 : 7$ at $T_0 = 298K$ and $p_0 = 10$ kPa, cell width 1.6 cm
- Similar configuration as E. Oran et al., J. Combustion and Flame 113, 1998
- Euler equations for 9 thermally perfect species, 34 elementary reactions
- Adaptation criteria:
  - *Scaled gradients of ρ and p*
  - *Error estimation in Y_i by Richardson extrapolation*
- 67.6 Pts within induction length. 4 additional refinement levels (2,2,2,4)

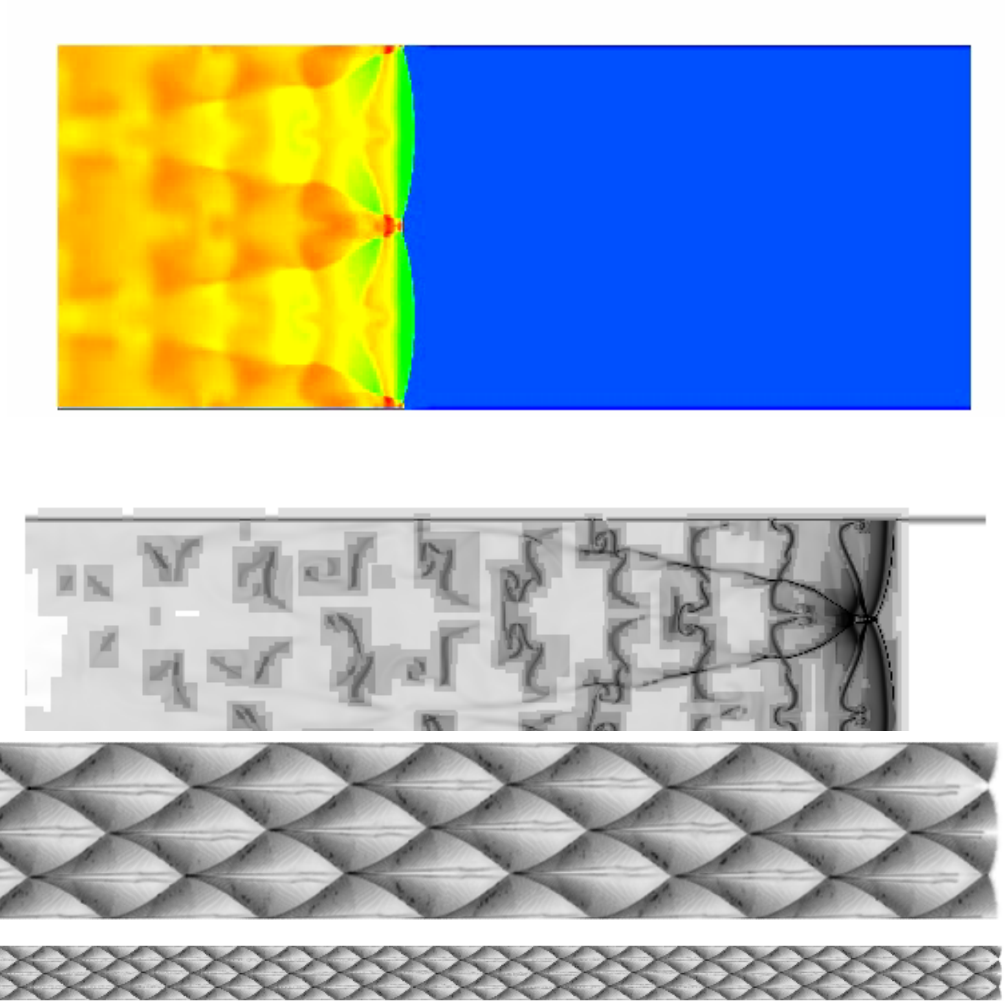

Detonation diffraction

- Detailed mechanism with 34 elementary reactions
- 25 Pts within induction length. AMR base grid 508x288, 4 additional levels (2,2,2,4)
- Adaptive computations use less than $3 \cdot 10^6$ cells instead of $150.8 \cdot 10^6$ cells (uniform grid)
- ~4000h CPU on 48 nodes Athlon 1.4 GHz

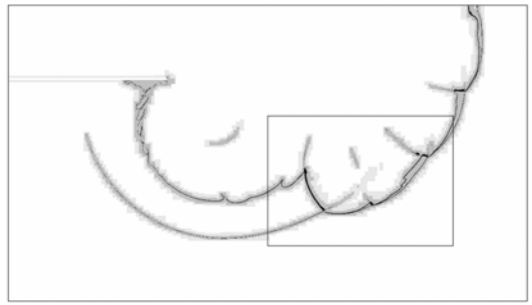

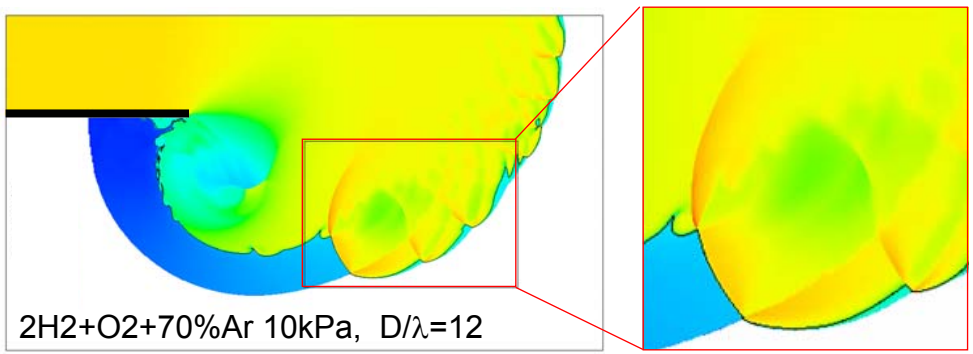

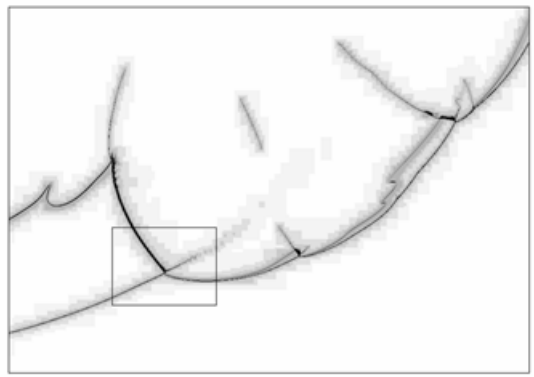

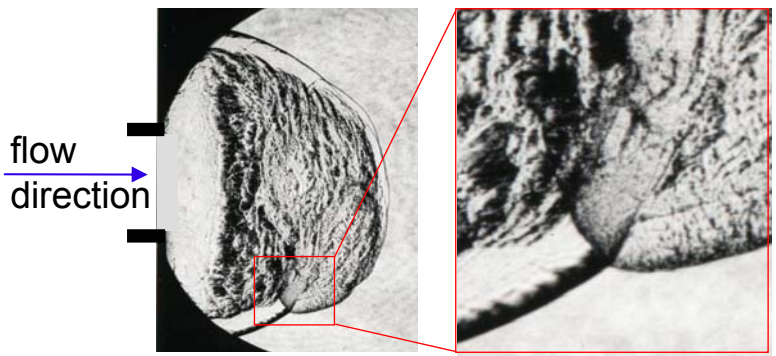

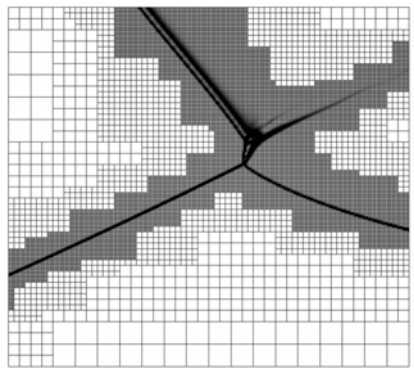

Detonation propagation through smooth pipe bends

- Same configuration as in 2D diffraction simulation. Tube width of 5 detonation cells (8 cm)
- Pipe bend with same radius. Angle: 15^o, 30^o, 45^o, 60^o
- 67.6 Pts within induction length. 4 additional refinement levels (2,2,2,4)
- Adaptive computations use $\approx 7 \cdot 10^6$ cells ($\approx 5 \cdot 10^6$ on highest level) instead of $1.2 \cdot 10^9$ cells (uniform grid)
- ~70,000h CPU on 128 CPUs Pentium-4 2.2GHz

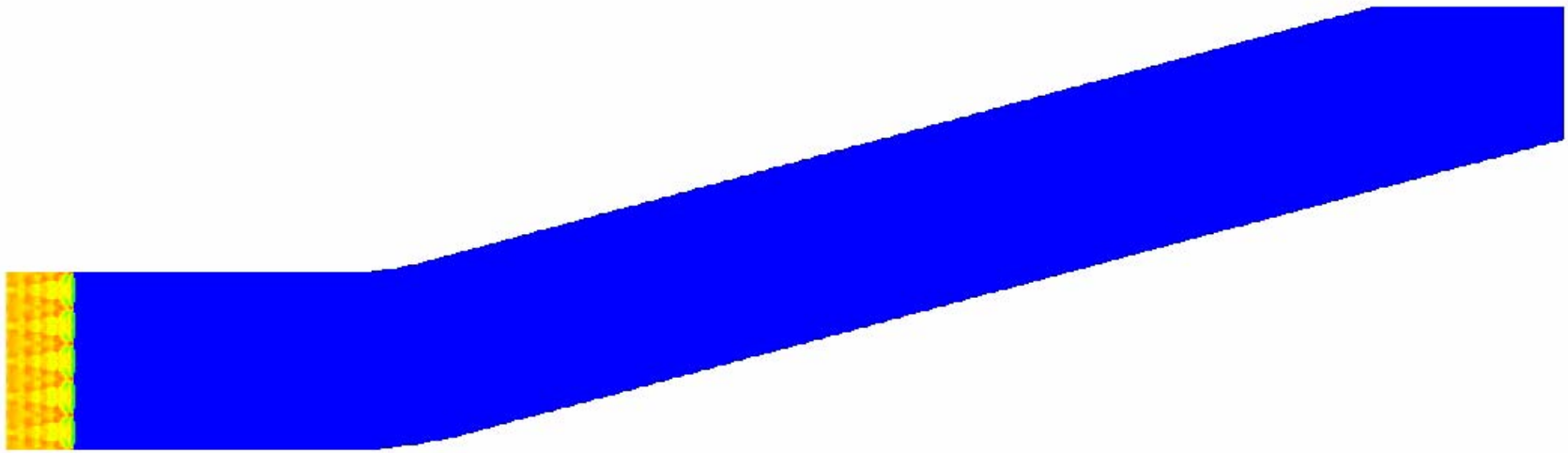

Color plot of temperature, 15^o pipe bend

Dynamic mesh adaptation: 60°

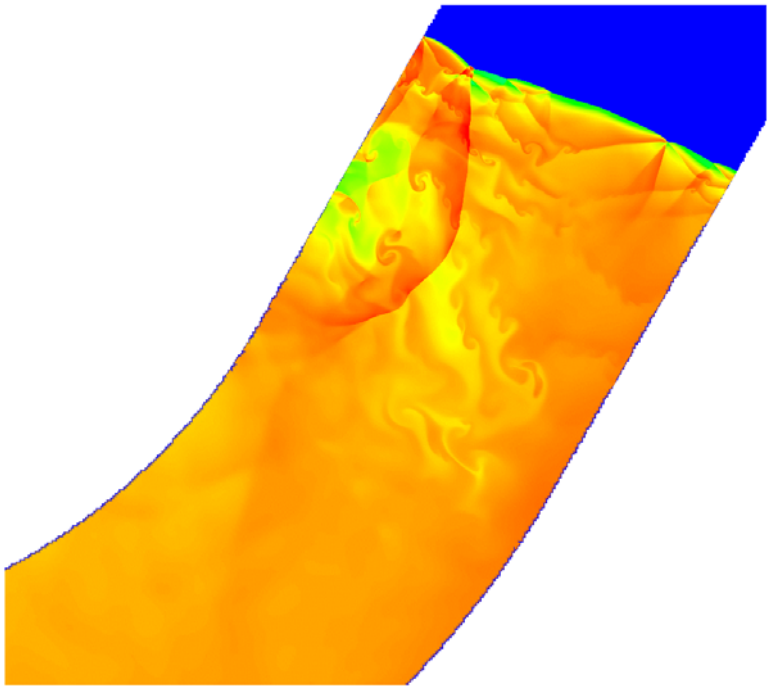

250 μs

Zoom into single triple point

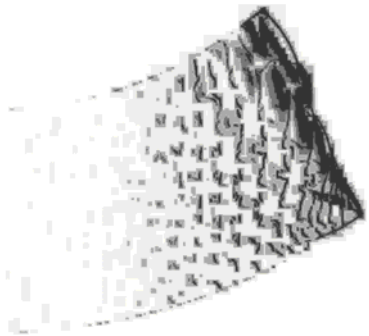

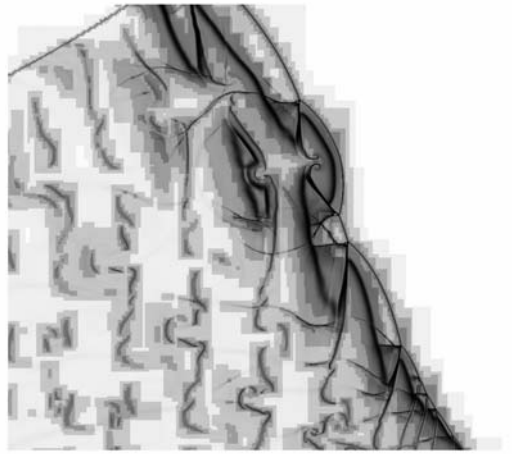

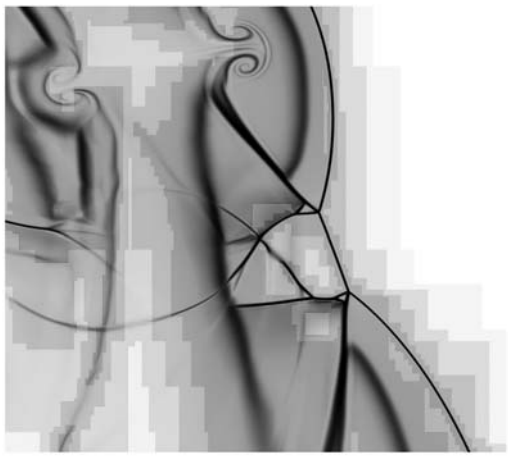

- Schlieren plot of density on 4 refinement levels.
- Savings from SAMR: 250 up to 680

Fluid-structure coupling (VTF)

- Couple compressible Euler equations to Lagrangian structure mechanics
- Compatibility conditions between inviscid fluid and solid at a slip interface
  - *Continuity of normal velocity:* $u^S_n = u^F_n$
  - *Continuity of normal stresses:* $\sigma^S_{nn} = -p^F$
  - *No shear stresses:* $\sigma^S_{n\tau} = \sigma^S_{n\omega} = 0$

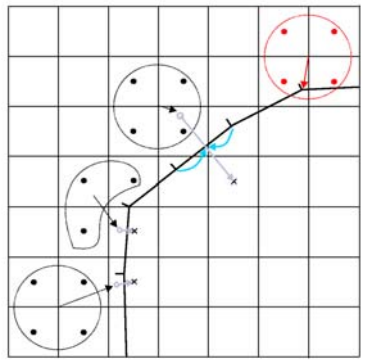

- Time-splitting approach for coupling
  - *Fluid:*
    - *Treat evolving solid surface with moving wall boundary conditions in fluid*
    - *Use solid surface mesh to update fluid level set on-the-fly with Closest-Point Tranform algorithm by S. Mauch (Caltech)*
    - *Use nearest velocity values* $\boldsymbol{u}^S$ *on surface facets to impose* u^F_n *in fluid*
  - *Solid:*
    - *Use interpolated hydro-pressure* p^F *to prescribe* σ^S_{nn} *on boundary facets*
- Ad-hoc separation in dedicated fluid and solid processors
  - *Parallel boundary data exchange library by S. Mauch*

- Elastic motion of a thin steel plate when being hit by a Mach 1.21 shock wave, Giordano et al. Shock Waves (2005)
- Steel plate modeled with finite difference solver using the beam equation

$$\rho h \frac{\partial^2 w}{\partial t^2} + EI \frac{\partial^4 w}{\partial x^4} = p(x,t)$$

- SAMR base mesh 320x64, 2 additional level with factors 2, 4

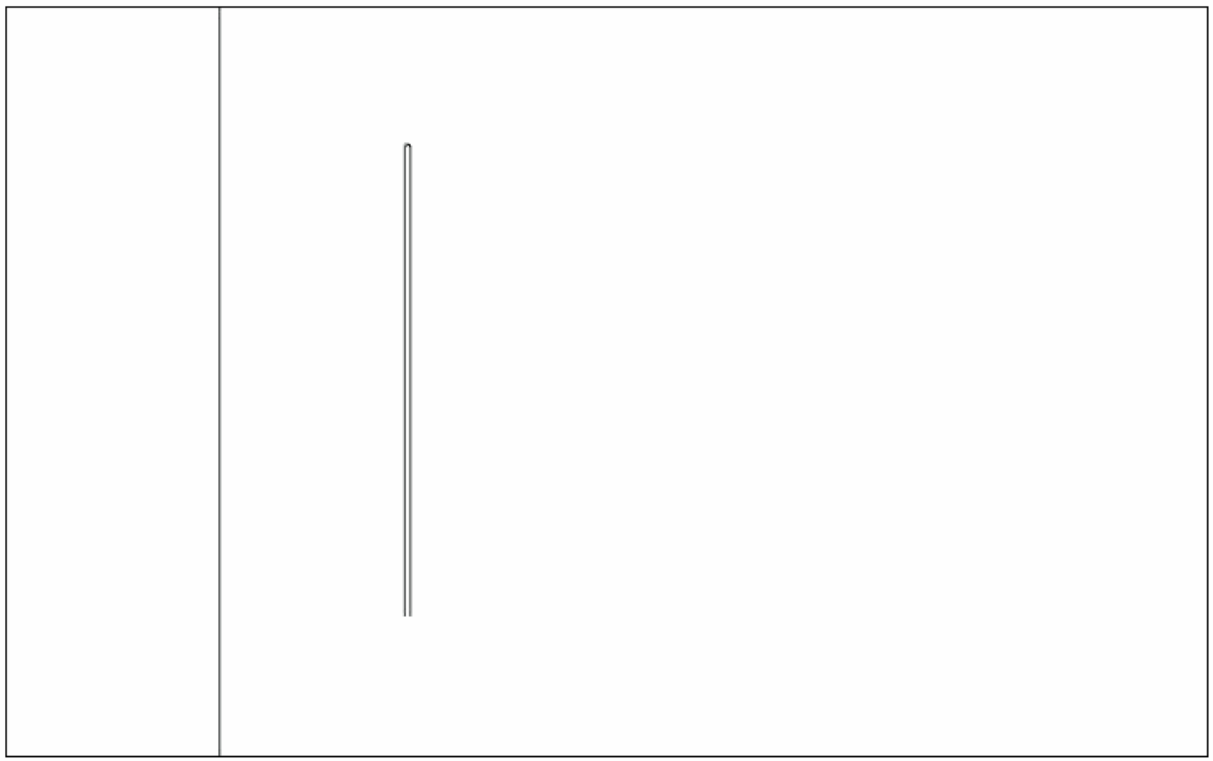

Schlieren plot of density

Multi-physics examples with fracture

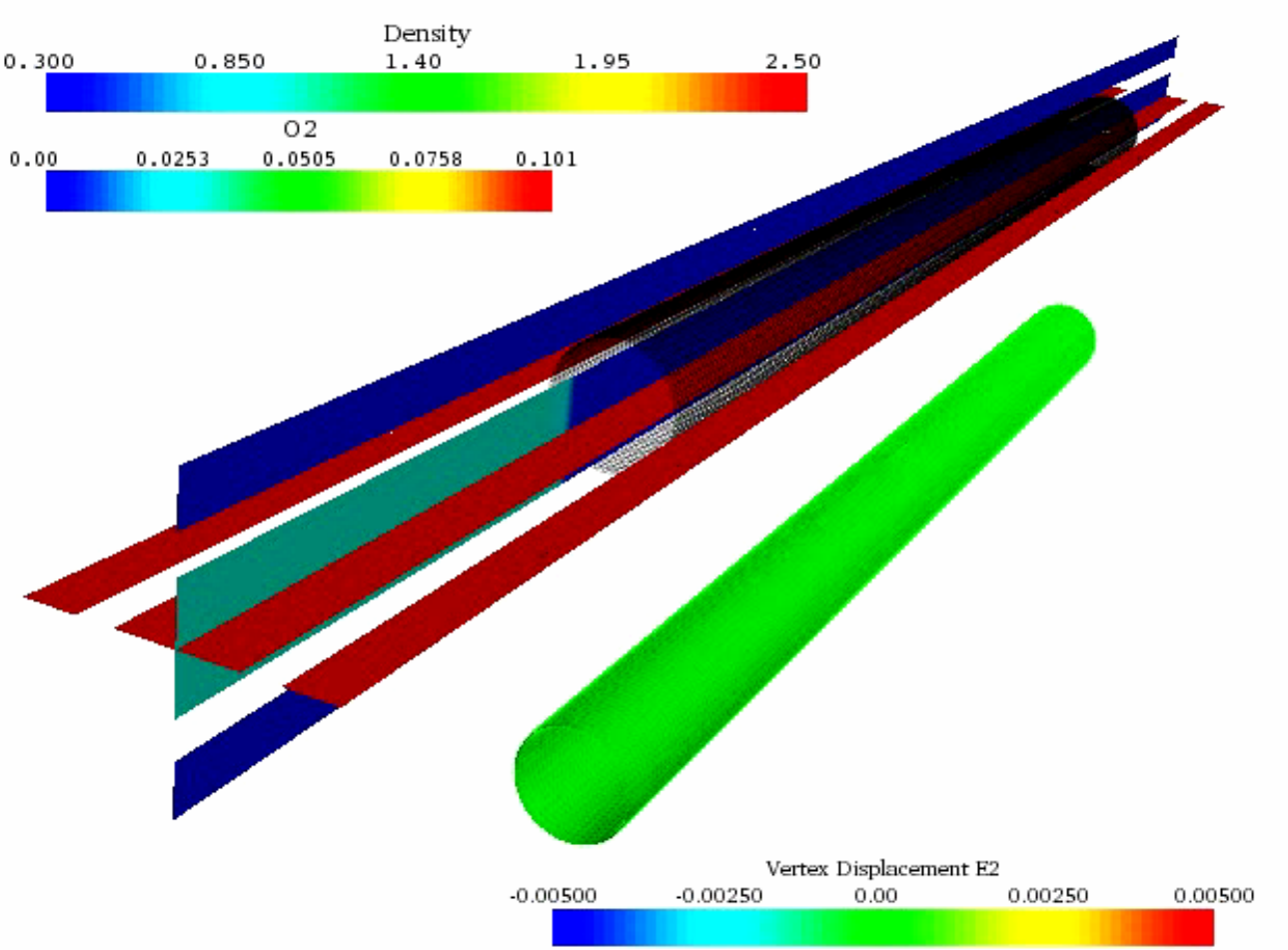

- *Thin aluminum test specimen embedded in shocktube (closed at upper end)*
- *Preflawed specimen ruptures from detonation wave in H_2-O_2 mixture ignited by shock wave reflection*
- *Specimen simulated by thin-shell FEM solver by F. Cirak (U Cambridge)*

Multi-physics examples with fracture

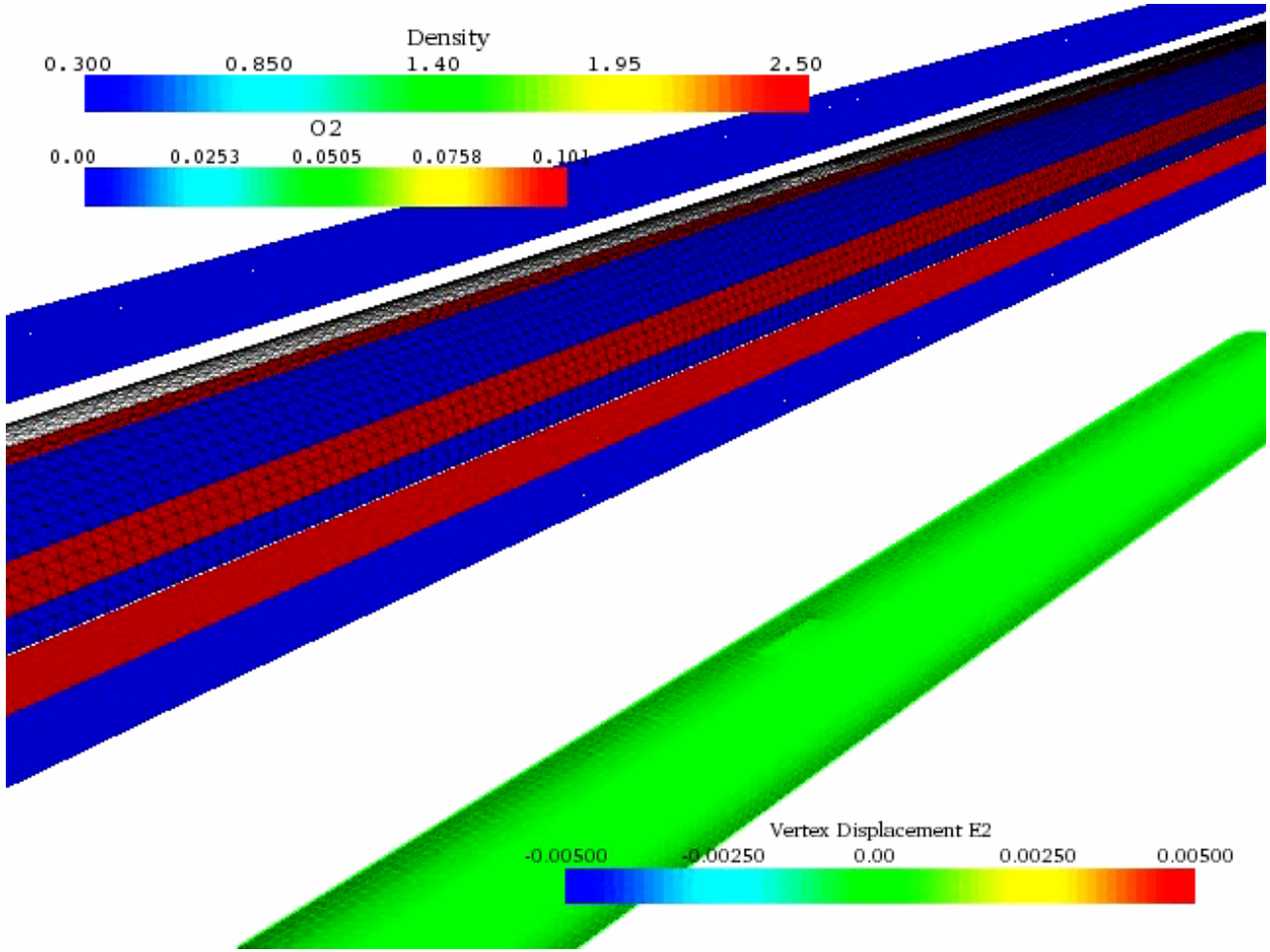

- *Detailed H_2-O_2 reaction mechanism*
- *Ignition and depletion visible from O_2 consumption*
- *6+10 nodes 2.2 GHz AMD Opteron quad processor, ca. 2300h CPU*

Conclusions

- Detailed construction of fully positivity-preserving upwind scheme for thermally perfect gas-mixtures
- Discussed embedding of this scheme into SAMR in a Cartesian ghost-fluid-type method
- Detonation structure simulations with detailed chemistry are possible nowadays in 2d
  - *Resolution down to the scale of secondary triple points can be provided in realistic geometries*
- Enabling components: Combining parallel SAMR with mixed explicit-implicit time operator splitting
  - *SAMR provides a sufficient spatial and temporal resolution*
  - *Saving from SAMR >50x for example for detonation diffraction simulations, up to >680x for pipe bend simulations*
  - *Operator splitting allows a cell-wise integration of stiff reaction terms*
    $\rightarrow$ no globally coupled implicit system
  - *Entire splitting scheme is time-explicit $\rightarrow$ time accurate, easy parallelization*
  - *High resolution finite volume schemes for homogeneous Euler equations and complex stiff ODE solvers can be reused*
  - *Distributed memory parallelization allows large-scale problems*
- Outlook: The Virtual Test Facility software
  - *Coupling of Lagrangian finite-element solvers to Eulerian SAMR-GFM framework Amroc for highly instationary fluid-structure interaction problems*
- Literature, links to software, etc. under *http://www.csm.ornl.gov/~r2v*

Abbreviations

- Amroc: Adaptive mesh refinement in object-oriented C++
- GFM: Ghost fluid method
- CPT: Closest point transform
- FEM: Finite element
- FV: Finite volume
- MUSCL: Monotone upstream-centered schemes for conservation laws
- ODE: Ordinary differential equations
- SAMR: Structured adaptive mesh refinement
- VTF: Virtual Test Facility